

AEROELASTIC AND CONTROL SYSTEM MODELING OF A MISSILE CONTROL FIN FOR AEROSERVOELASTIC ANALYSIS

Mehmet Ozan Nalci¹
Roketsan Missile Industries Inc.
Ankara, Turkey

Altan Kayran²
Middle East Technical University
Ankara, Turkey

ABSTRACT

In this study; the structural, aerodynamic and servo-actuation system models are built for integration into a generic aeroservoelastic model of a typical missile control fin with an electromechanical actuator. Linear models of the control fin structure, aerodynamics and servo-actuation system are built, in order to be able to analyze the aeroservoelastic system both in frequency and time domain. Structural and aerodynamic modeling are performed in MSC PATRAN and MSC FlightLoads and Dynamics respectively. The information about the structure and the aerodynamics of the missile control fin is extracted from MSC NASTRAN solvers in matrix format, so that the aeroelastic equation of motion can be reformulated in MATLAB as a state space model. In order to be able to verify this interfacing step; normal modes analysis and flutter analysis are performed with both MSC NASTRAN and MATLAB. The unsteady, single frequency, "Generalized Aerodynamic Force" matrices obtained from MSC FlightLoads and Dynamics are input to a rational fraction approximation method, so that the aerodynamic forces are represented in the continuous frequency domain. An electromechanical servoactuation system model is developed in MATLAB for controller design. A DC Motor and a transmission unit are selected for the smooth operation of the servo-actuation system, in compliance with given time response requirements. A PD controller synthesis is then carried out using the Root Locus Method. The PD controller design is carried out by neglecting the elastic structural and unsteady aerodynamic effects on the fin, as if the fin is rigid and the aerodynamics is steady.

INTRODUCTION

The vast majority of problems regarding the flexibility of missiles are focused on control surfaces such as fins or canards, since the slenderness of these control surfaces are more pronounced than that of the missile body. Moreover, the interaction of structural dynamics with control system dynamics renders the control surface design and analysis more intriguing due to the frequency separation between structural and control system dynamics being relatively narrow and the motion feedback sensors having high enough bandwidth to measure flexible motion. On the contrary, the motion due to flexible modes of the missile body are usually filtered by the bandwidth of onboard inertial measurement units and the control command generating autopilots during flight, resulting in less interaction with the overall missile control system.

Structural modeling of aircraft structures for linear aeroelastic analysis has long been performed by utilizing the finite element method[Bisplinghoff, Raymond L., Ashley, H., Halfman, Robert L., 1957]. Formulating the structural dynamics of the missile control fin with finite element modeling renders the aeroservoelastic model to be applicable to complex geometries of various shapes and boundary conditions. Subsonic aerodynamic modeling of slender lifting surfaces on the other hand, is commonly carried out by utilizing the linearized potential flow equations, when the flow is confined to small incidence angles[Gülçat, Ü., 2010]. MSC FlightLoads and Dynamics module includes a subsonic

¹ Senior Modeling and Simulation Engineer in Roketsan Missile Inc., Email: onalci@roketan.com.tr

² Professor at Department of Aerospace Engineering, Email: akayran@metu.edu.tr

aerodynamic solver, which solves the linearized potential flow equation for arbitrary geometries by panel discretization. The Doublet Lattice Method (DLM), which is an acceleration potential method developed by Albano and Rodden [Albano, E., and Rodden, W. P., 1969] is implemented in the solver to model the unsteady lift generation on the panels due to harmonic structural motion. The DLM can also be used for modeling the steady aerodynamics when the reduced frequency is very close to zero. It is actually equivalent to the Vortex Lattice Method [Luis R. Miranda, Robert D. Elliott, and William M. Baker, 1977] when the reduced frequency is zero. The DLM creates the so called Generalized Aerodynamic Forcing (GAF) Matrices at specified Mach numbers and reduced frequencies for simple harmonic motion of the structure. In order to model the transient aerodynamic phenomena together with the steady state aeroelastic condition, the frequency dependent GAF matrices are represented as a continuous function of reduced frequency. For a specified Mach number and several reduced frequencies obtained by the DLM, it is possible to obtain a continuous frequency response by utilizing Rational Function Approximation (RFA) methods [Vepa, R., 1976.]. Roger's Method [Roger, K. L., 1977] and Minimum State Approximation Method of Karpel [Karpel, M., and Hoadley, S. T., 1991] are most widely used tools for rational function approximation of oscillatory aerodynamic forces. Modeling the structural dynamics and aerodynamics with finite element methods renders possible the analysis of the aeroelastic system by modal discretization. The control mode approach [Karpel, M., 1999] renders possible the application of control action to the aeroelastic system by modal superposition of the elastic modes and the rotational rigid body mode of the fin, such that the inertial and aerodynamic interaction between the modes can be studied.

METHOD

The motivation behind this study is to build structural, aerodynamic and servoa ctuation system models, which could be integrated to form a linear aeroservoelastic mathematical model of an all-movable aerodynamic control surface. Through the modeling process, the aim is to obtain the parameters of the second order linear differential equation given in Eqn. (1), governing the aeroelastic dynamics of the missile control fin.

$$\left(s^2 [\mathbf{M}_{mm}] + s [\mathbf{C}_{mm}] + [\mathbf{K}_{mm}] - q [\bar{\mathbf{Q}}_{mm}(M, s)] \right) \{ \zeta_m(s) \} = \{ T_{act}(s) \} \quad (1)$$

In Eqn. (1), \mathbf{M}_{mm} is the modal mass matrix, \mathbf{C}_{mm} is the modal damping matrix and \mathbf{K}_{mm} is the modal stiffness matrix; which are all obtained from the finite element model of the fin. ζ_m is the aeroelastic generalized coordinate vector, which is the independent variable to be solved for. The aerodynamic forcing vector that act on the structure is described as a function of the generalized aerodynamic matrices \mathbf{Q}_{mm} , which also includes the aerodynamic force generated by the control mode (the rotational rigid body mode of the fin), and the external control moment $T_{act}(s)$ that is applied to the fin by the servoa ctuation system. The mass, stiffness and aerodynamic matrices in the formulation are obtained from the models built in MSC Patran and MSC Flightloads and Dynamics, using the normal modes and aeroelasticity solvers of MSC NASTRAN. The matrices obtained are given as input to the Matlab codes that model the aeroservoelastic system [Nalci, O., Kayran, A., 2013]. Finally a state space system in the form of Eqn. (2) is obtained.

$$\{ \dot{z}(t) \} = [\mathbf{A}_{sys}] \{ z(t) \} + [\mathbf{B}_{sys}] \{ u(t) \} \quad (2)$$

In order to verify the interfacing steps between MSC Nastran and Matlab, normal modes analysis and flutter analysis are carried out in both software platforms. The p-k method in MSC Nastran, root locus method and time domain method in Matlab are utilized for flutter solutions. The normal modes analysis is performed by the classical eigenvalue problem solution, with both software platforms.

A servoa ctuation system is augmented to the aeroelastic system given in Eqn. (2), so that the interaction between the control dynamics and the aeroelastic dynamics of the fin can be studied. The servoa ctuation system is comprised of a PD controller and a DC Motor – Transmission assembly . The servoa ctuation system design includes the specification of inertial and external aerodynamic moments as input, selecting the proper DC Motor - Transmission assembly, and designing a controller for performance and stability requirements of the resulting closed loop system. The existence of aeroelastic dynamics is neglected throughout the design process. The PD controller synthesis is

carried out using the Root Locus Method. Performance of the servoa ctuation system is verified in the absence of aeroelastic dynamics, with regard to specified performance requirements. The output of the servoa ctuation system model is the input of Eqn. (2). The aeroservoelastic modeling methodology followed is given in Figure 1.

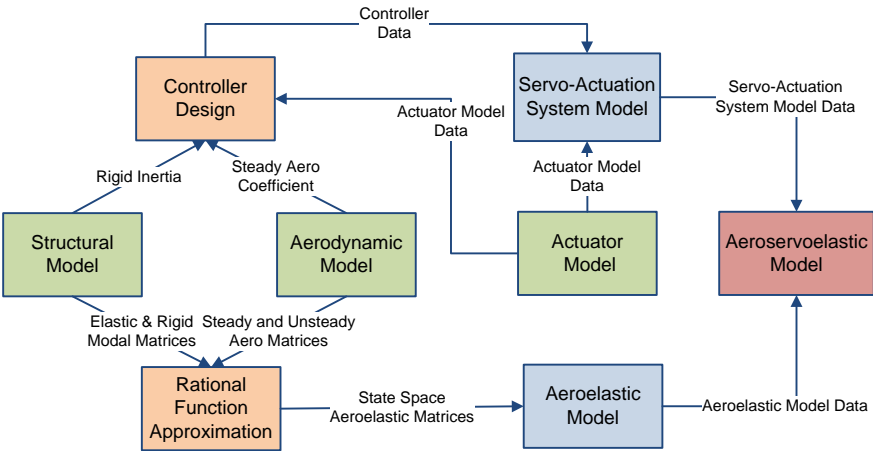


Figure 1 Methodology of Aeroservoelastic Modeling

Structural Model

The missile control fin that is studied is tightly connected to the servo-actuation system by a shaft. The servo-actuation system is assumed to be composed of a DC Motor and a transmission unit. The connection between the fin and the transmission unit and the thickness distribution of the fin are depicted in Figure 2 and Figure 3 respectively.

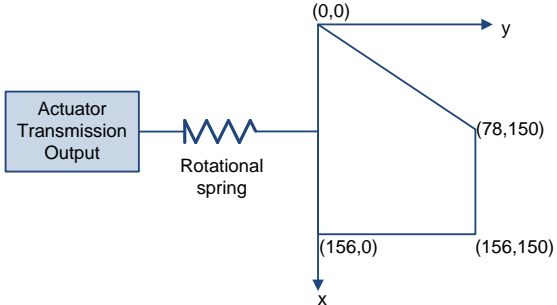


Figure 2 Transmission-Fin Connection

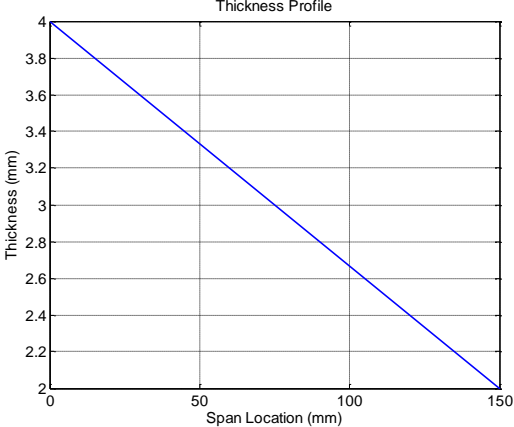


Figure 3 Thickness distribution of the control fin

Two finite element models are prepared for distinct purposes. The first finite element model (FN1) is prepared for the p-k method of flutter analysis, and normal modes analysis for the elastic modes in MSC Nastran. In this model, the fin is connected to the actuator through a shaft. This shaft is assumed to be rigid in all five degrees of freedom except for the rotational degree of freedom in the y-axis shown in Figure 4. It is assumed that the shaft reflects the resultant static stiffness of the actuator and the connecting shaft. In the y-axis, it has a stiffness of 120 N.m/rad. To model this shaft connection, a point on the ground is generated such that it is fixed in all degrees of freedom. The mid-node on the root chord of the fin is rigidly connected to this point through a multi point constraint (MPC), such that all five degrees of freedom except the rotational one in y-axis is fixed for this node. The rotational stiffness of the shaft in y-axis is modeled by a one dimensional bar element which has no mass or inertia. The model is shown in Figure 4, where Element 43 is the bar element. The fin structure is modeled with 42 QUAD4 elements.

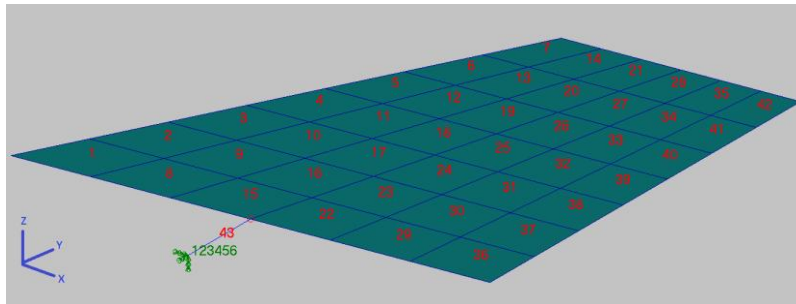


Figure 4 Finite Element Model FN1

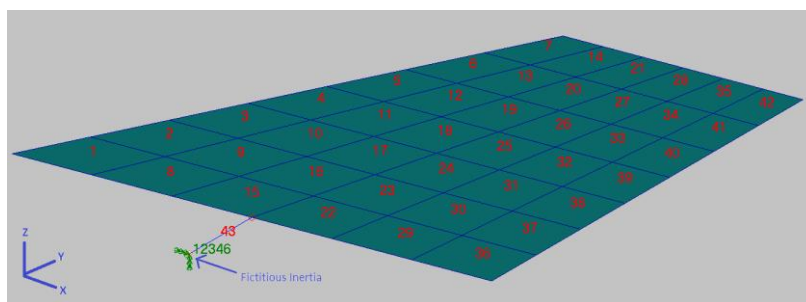


Figure 5 Finite Element Model FN2

A second model (FN2) is prepared, so that the rigid body mode could be obtained together with the elastic modes, without affecting the mode shapes and natural frequencies of the elastic modes. The rigid body mode is generated so that it is used for modeling the rigid control motion of the actuator. For this purpose, the boundary condition on the point on the ground is modified such that it is disconnected from the ground in the y-axis rotational degree of freedom. However, in this case, the mode shapes and the frequencies of the elastic modes are changed. To generate the needed modes in a single normal modes analysis run in MSC Nastran, a very high fictitious inertia is used in the y-axis, to mimic the fixed boundary condition at the point on the ground. The fictitious inertia is about 10^6 times greater than that of the rotational inertia of the fin. The high inertia adds a huge inertial resistance to the motion at the point where it is added. Therefore, the mode shapes and natural frequencies contain a rigid body mode, in addition to the original elastic modes and frequencies obtained from the model FN1. The mass matrix \mathbf{M}_{mm} is now changed, but the additional inertia is discarded from \mathbf{M}_{mm} when it is used in subsequent aeroelastic analysis in Matlab. The model is shown in Figure 5, together with the changed boundary condition and the node where the fictitious inertia is added. CMASS1 element is used for the added inertia, and a SUPORT statement is inserted into the Bulk Data Section of MSC Patran flutter analysis menu [Rodden, W.P., and Johnson, E. H., 1994], so that the rigid body mode obtained has exactly zero natural frequency. The modes taken into account for the aeroelastic analysis are limited by an upper limit of 1000 Hz. Normal modes analysis of both models are performed by Nastran, and the comparison of the natural frequencies is given in Table 1 for the 5 elastic modes besides the rigid body rotation mode.

Table 1 Comparison of natural frequencies determined by finite element models FN1 and FN2

	Model FN1	Model FN2
Rigid Body Mode	-	0.0000
Elastic Mode 1	86.8891	86.8891
Elastic Mode 2	159.6022	159.6022
Elastic Mode 3	566.0895	566.0895
Elastic Mode 4	627.1564	627.1564
Elastic Mode 5	972.5351	972.5351

As observed from Table 1, the fictitious inertia worked perfectly, and the results obtained for the elastic natural frequencies of models FN1 and FN2 are identical. Figure 6 shows the first four elastic mode shapes.

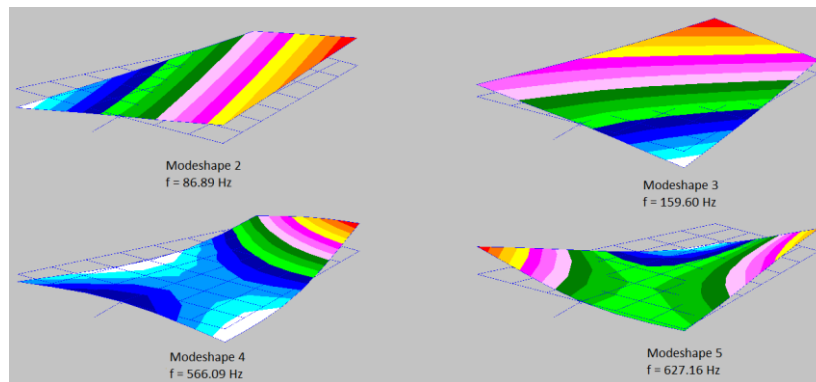


Figure 6 Elastic Modeshapes 1-to-4

An additional normal modes analysis is carried out in MATLAB, so that the matrices, which are extracted from MSC NASTRAN using the DMAP codes [Reymond, M., 2006] inserted, are verified. In MATLAB, the eigenvalue problem solver function 'eig'¹⁵ is used to obtain natural frequencies and mode shapes. For the model FN2, natural frequencies obtained from MATLAB are presented together with the results of MSC NASTRAN in Table 2.

Table 2 Natural Frequency Comparison of MSC Nastran and MATLAB Modal Analyses

	Model FN2	Model FN2
Rigid Body Mode	0.0000	1.52691E-07
Elastic Mode 1	86.8891	86.8891
Elastic Mode 2	159.6022	159.6022
Elastic Mode 3	566.0895	566.0895
Elastic Mode 4	627.1564	627.1564
Elastic Mode 5	972.5351	972.5351

Since the modes are identical, the stiffness and mass matrices \mathbf{K}_{mm} and \mathbf{M}_{mm} obtained from MSC NASTRAN and implemented in MATLAB are used in further aeroelastic analysis with confidence. Note that the modal damping matrix \mathbf{C}_{mm} can be set to zero for the sake of simplicity, as its effect on the response is usually insignificant when aerodynamic damping forces are present.

Aerodynamic Model

Aerodynamic modeling of aircraft structures, necessitates a very careful treatment of the underlying physical phenomena. The operating conditions of the missile control fin, such as given in Table 3 should be considered, in order to make physically sound assumptions about the flow.

Table 3 Flight Conditions of the Missile Control Fin

	Minimum	Maximum
Range of Altitudes	0 m	5000 m
Range of Mach Numbers	0.4	0.6
Range of Incidence Angle	-15°	+15°

The flight conditions given in Table 3 implies that the flow around the control fin is subsonic and compressible. Furthermore, the aerodynamics can be assumed to be linear in the incidence angle region that is specified [Anderson, J. D., 2001]. An additional assumption, that the flow is inviscid leads to the well known DLM for unsteady flow, where the final assumption is justified by the fact that viscous effects have little effect on the lift on the fin in the relatively small incidence region. Aerodynamic modeling of the missile control fin can therefore be carried out in MSC Flightloads and Dynamics, with the DLM, for obtaining the unsteady GAF matrices for a predefined region of reduced frequency at certain Mach numbers. The GAF matrices Q_{nm} are then given as input to Roger's RFA method, so that the aerodynamic forces are represented in the continuous frequency domain. To verify the GAF matrices' implementation to the MATLAB codes developed, flutter analysis in both MSC NASTRAN and MATLAB are performed.

The Doublet Lattice Modeling of the missile control fin aerodynamics requires certain rules to be followed in MSC Flightloads and Dynamics. Two of them significantly affect the accuracy of aerodynamic forcing and subsequent aeroelastic analysis [Rodden, W.P., and Johnson, E. H., 1994]. There should be a minimum of 15 boxes (panels) per wavelength for each chord strip. Not less than four boxes per chord should be used. Furthermore, boxes (panels) should maintain an aspect ratio of less than 3 in the default Doublet-Lattice formulation. The parameter 'boxes per wavelength' is defined as $BPW = U_{min} / f_{max} \Delta x$ where, Δx is the chord length of a single panel of the aerodynamic surface at a strip. U_{min} is the minimum airspeed, and f_{max} is the maximum structural frequency that are used in the analysis. Panel discretization of the fin surface is shown in Figure 7 together with the 'boxes per wavelength' criterion and in Figure 8 together with the 'aspect ratio' criterion. For the model obtained, both criteria are satisfied.

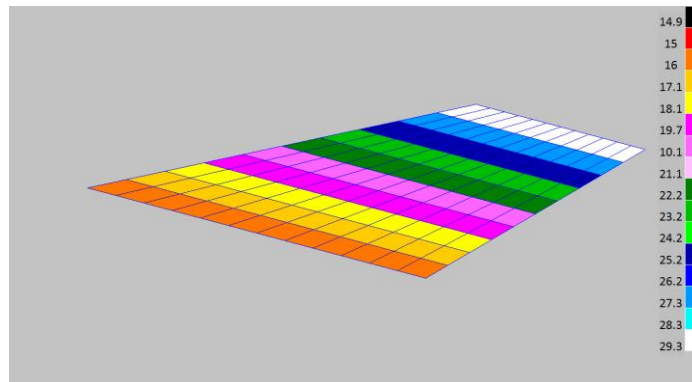


Figure 7 Aerodynamic Mesh – Boxes per Wavelength

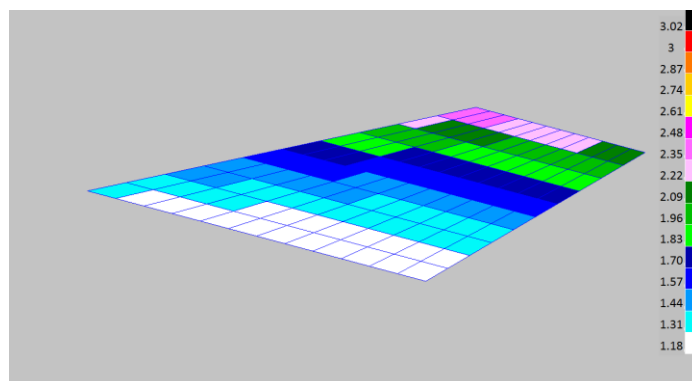


Figure 8 Aerodynamic Mesh – Aspect Ratio

Figure 9 shows the DMAP code inserted to the Executive Control Deck to output the GAF Matrices at different reduced frequencies and at a single Mach number to a text file. This text file is read by MATLAB with an interfacing code developed. The GAF matrices are output in the k-set, which is the aerodynamic grid point set in MSC Nastran [Rodden, W.P., and Johnson, E. H., 1994].

```

$ Direct Text Input for Executive Control
COMPILE FLUTTER $
ALTER 31 $
OUTPUT4 GPIK,GDKI,GDAK,,//0/21 ///30 $ OUTPUT4 QKK,,,,//0/21 ///30 $
FILE QKKL=APPEND
ALTER 'delete /qhh,qhj,qkh'
MATGEN ,/I240/1/240 $
amp      ajj0,wskjf,d1jk,d2jk,I240,I240,I240,d1je,d2je,
          mklist,lajjt,uajjt/
          QKK,obsi,obsii/240/noue/gustaero/machno/kbar $
APPEND QKK,/QKKL/2
ALTER 'ENDIF $ NOQHHL>0'
OUTPUT4 QKKL,,,,//0/21 ///30 $

```

Figure 9 DMAP Code in Executive Control Deck for GAF Matrix Extraction

Rational Function Approximation to Unsteady Aerodynamics:

Aeroservoelastic formulation of the missile control fin requires transient aerodynamic effects to be modeled. The GAF matrices obtained from DLM cannot be directly used to model transient aerodynamic phenomena, since DLM is only directly applicable to steady state sinusoidal motion. All RFA methods depend on least square techniques, which fit a frequency response function to GAF matrices at multiple reduced frequencies. Comparisons of accuracy and computational efficiency between these methods are available in literature [Karpel, M., 1982]. Roger's Method approximates the unsteady aerodynamics with following frequency response function that depends on reduced frequency and Mach number:

$$[\bar{\mathbf{Q}}(M, k)] = [\mathbf{A}_0] + (ik)[\mathbf{A}_1] + (ik)^2[\mathbf{A}_2] + \sum_{n=1}^N \frac{(ik)[\mathbf{A}_{n+2}]}{ik + \beta_n} \quad (3)$$

β : Roots of Aerodynamic Lag Functions

N : Number of Aerodynamic Lag States

In Eqn. (3), $\mathbf{A}_{0...N+2}$ are the constant matrices to be determined from least square approximation for the best fit of $\mathbf{Q}(M, k)$. β_n are the aerodynamic lag roots. β_n are preset to specific values in the frequency range of interest, so that the aerodynamic lag functions are stable, the least square problem becomes linear, and the fit is satisfactory. Note that for each element of $\mathbf{Q}(M, k)$ at different frequencies $\mathbf{Q}^{ij}(M, k_1), \mathbf{Q}^{ij}(M, k_2) \dots \mathbf{Q}^{ij}(M, k_{n_k})$, a least square fit is generated. Given a $\mathbf{Q}(M, k)$ matrix of size n_m at a Mach number, the number of linear least square fits required is $n_m^2 \times n_k$, where n_k is the number of GAF matrices at n_k different reduced frequencies. β_n are the same for each fit, so that the size of the resulting aeroelastic equation is kept small. By modeling the unsteady aerodynamics with Roger's Method, number of states of the resulting aeroelastic equation will be $n_s(N+2)$, where n_s is the number of elastic modal degrees of freedom. To calculate $\mathbf{A}_{0...N+2}^{ij}$ for a Mach number, $\bar{\mathbf{Q}}^{ij}(M, k)$ is divided into real and imaginary parts such that:

$$[\bar{\mathbf{Q}}^{ij}(M, k)] = [\bar{\mathbf{Q}}_R^{ij}(M, k)] + i[\bar{\mathbf{Q}}_I^{ij}(M, k)] \quad (4)$$

$$[\bar{\mathbf{Q}}_R^{ij}(M, k)] = [\mathbf{A}_{0}^{ij}] - k^2[\mathbf{A}_{2}^{ij}] + \sum_{n=1}^N \frac{k^2[\mathbf{A}_{n+2}^{ij}]}{k^2 + \beta_n^2} \quad (5)$$

$$[\bar{\mathbf{Q}}_f^{ij}(M, k)] = k[\mathbf{A}^{ij}_1] + \sum_{n=1}^N \frac{\beta_n k [\mathbf{A}^{ij}_{n+2}]}{k^2 + \beta_n^2} \quad (6)$$

Then these parts are written in matrix form, for each Mach - reduced frequency pair:

$$[\bar{\mathbf{Q}}_R^{ij}(M, k_f)] = \{K_{Rf}\} [\mathbf{A}^{ij}] \quad (7)$$

$$[\bar{\mathbf{Q}}_I^{ij}(M, k_f)] = \{K_{If}\} [\mathbf{A}^{ij}] \quad (8)$$

where K_{Rf} , K_{If} and \mathbf{A}^{ij} are defined as:

$$K_{Rf} = \begin{bmatrix} 1 & 0 & -k_f^2 & \frac{k_f^2}{k_f^2 + \beta_1^2} & \frac{k_f^2}{k_f^2 + \beta_2^2} & \cdots & \frac{k_f^2}{k_f^2 + \beta_N^2} \end{bmatrix} \quad (9)$$

$$K_{If} = \begin{bmatrix} 0 & k_f & 0 & \frac{\beta_1 k_f}{k_f^2 + \beta_1^2} & \frac{\beta_2 k_f}{k_f^2 + \beta_2^2} & \cdots & \frac{\beta_N k_f}{k_f^2 + \beta_N^2} \end{bmatrix} \quad (10)$$

$$\mathbf{A}^{ij} = [\mathbf{A}^{ij}_0 \quad \mathbf{A}^{ij}_1 \quad \mathbf{A}^{ij}_2 \quad \mathbf{A}^{ij}_3 \cdots \mathbf{A}^{ij}_{(N+2)}]^T \quad (11)$$

Then the following complex error function is defined for linear least square minimization problem:

$$[\mathbf{E}^{ij}(M, k_f)] = [\mathbf{Q}^{ij}(M, k_f)] - [\bar{\mathbf{Q}}^{ij}(M, k_f)] \quad (12)$$

The aim is to make a linear least square fit, so that the left hand side of Eqn. (12) is minimized. Then,

$$\frac{\partial}{\partial \mathbf{A}^{ij}_f} \sum_{n=1}^{n_k} (\mathbf{E}^{ij}(M, k_f) \mathbf{E}^{ij}(M, k_f)') = 0 \quad (13)$$

Eqn. (13) is solved to obtain Eqn. (15).

$$\mathbf{A}^{ij} = \left[\sum_{f=1}^{n_k} \{K_{Rf}\}^T \{K_{Rf}\} + \{K_{If}\}^T \{K_{If}\} \right]^{-1} \sum_{f=1}^{n_k} [\mathbf{Q}_{Rf}] \{K_{Rf}\}^T + [\mathbf{Q}_{If}] \{K_{If}\}^T \quad (14)$$

When all \mathbf{A}^{ij} is calculated for each element of $\bar{\mathbf{Q}}(M, k)$, one obtains a fit with respect to reduced frequency k . In order to use $\bar{\mathbf{Q}}(M, k)$ in time domain simulations and frequency domain analysis, it is expressed in Laplace domain, using the relation $ik = sb/U$, as shown in Eqn. (16).

$$[\bar{\mathbf{Q}}(M, s)] = [\mathbf{A}_0] + \frac{sb}{U} [\mathbf{A}_1] + \left(\frac{sb}{U}\right)^2 [\mathbf{A}_2] + \sum_{n=1}^N \frac{s[\mathbf{A}_{n+2}]}{s + \frac{U}{b} \beta_n} \quad (15)$$

GAF matrices are obtained from MSC Nastran in the aerodynamic set, namely the k-set. The matrices are then transformed to the m-set as shown in Eqn. (17) and Eqn. (18), where \mathbf{G}_{ka} and ϕ_{am} are the spline matrix matrix between the structural and aerodynamic grid points, and the reduced modal matrix respectively.

$$[\mathbf{Q}^{ij}_{aa}] = [\mathbf{G}^T_{ka}] [\mathbf{Q}^{ij}_{kk}] [\mathbf{G}_{ka}] \quad (16)$$

$$[\mathbf{Q}^{ij}_{mm}] = [\phi^T_{am}] [\mathbf{Q}^{ij}_{aa}] [\phi_{am}] \quad (17)$$

Then Roger's method is applied on the m-set GAF matrices to obtain $\bar{\mathbf{Q}}_{mm}(M, s)$. In Eqn. (15), the number of aerodynamic lag roots is determined so that a satisfactory fit for GAF matrices is performed. Typically 2 to 4 lag roots are used in aeroelastic studies[Karpel, M., 1982]. The aerodynamic forcing in Laplace domain is finally expressed as in Eqn. (19).

$$\{\mathbf{F}_m(s)\} = q[\bar{\mathbf{Q}}_{mm}(M, s)]\{\zeta_m(s)\} \quad (18)$$

In Figure 10 and Figure 11, an element of $\bar{\mathbf{Q}}_{mm}$ and \mathbf{Q}_{mm} are compared for each reduced frequency at which \mathbf{Q}_{mm} is obtained. In Figures 10 and 11, estimated elements of the GAF matrices are obtained by applying the Roger's RFA to the GAF Matrices at Mach 0.6.

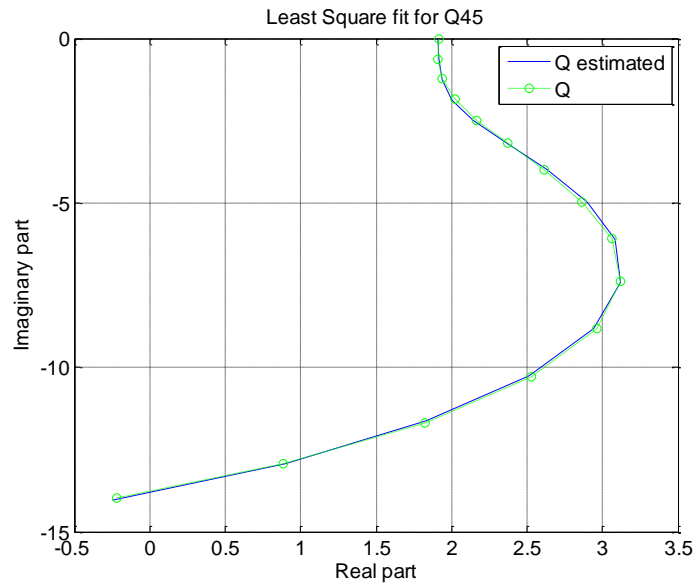


Figure 10 RFA Fit for \mathbf{Q}_{45}

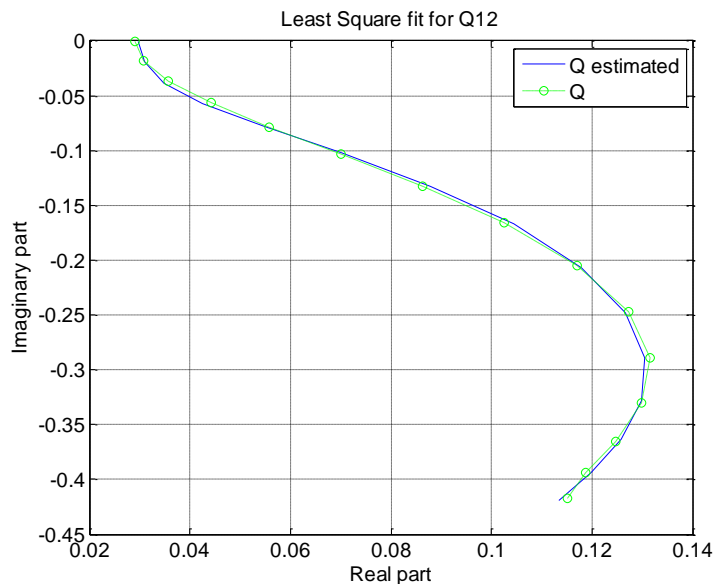


Figure 11 RFA Fit for \mathbf{Q}_{12}

Flutter Solution Methods

There are various flutter solution techniques for aeroelastic systems in literature. The most frequently used methods for linear systems that can be represented in frequency domain are the k-method and

the p-k method. Commercial programs like ZAERO and MSC Nastran also include the g method and the k-e method respectively. P-k method is selected as a frequency domain solution method because of its ease of use, and accuracy. Analysis carried out in MSC Nastran includes only the p-k method solution. On the other hand, in Matlab, by utilizing state space system matrix obtained in Eqn. (2), the root locus solutions are obtained. To calculate the flutter speed, a time domain simulation which has a non-zero initial condition, is also performed in Matlab. The results obtained in both software platforms are presented, and the aeroelastic model developed in the Matlab environment is verified. .

P-k Method Solution:

The matched point results of the flutter analysis carried out at three different altitudes with the p-k method are presented in Table 4. The methodology of followed in application of the p-k method in MSC Flight Loads and Dynamics can be found in [Nalci, O. , 2013].

Table 4 Flutter Analysis Results

Analysis Altitude (m)	0	2500	5000
Flutter Point	Aeroelastic Mode 2	Aeroelastic Mode 2	Aeroelastic Mode 2
Flutter Speed (m/s)	251.12	256.62	292.81
Flutter Frequency (Hz)	143.55	143.57	143.57
Equivalent Airspeed (m/s)	251.12	251.04	251.21
Equivalent Mach #	0.74	0.76	0.78

The mode at which flutter occurs is presented in Figure 12. Airspeed vs. damping coefficient and airspeed vs. frequency plots are provided in Figure 13 and Figure 14 respectively, for sea level flutter analysis.

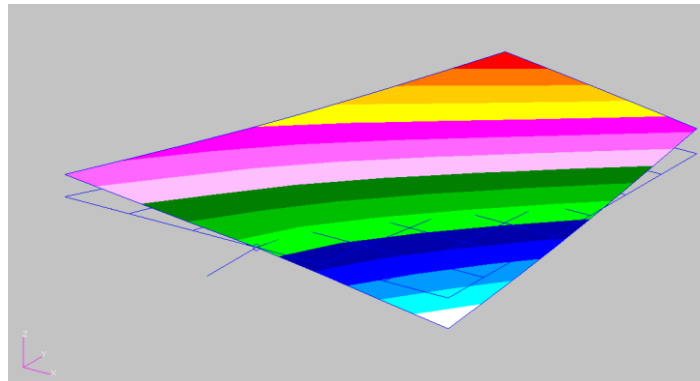


Figure 12 Flutter Modeshape

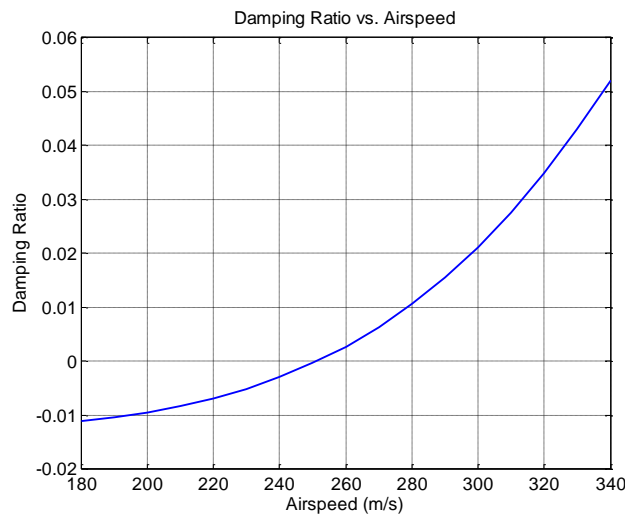


Figure 13 Damping Ratio of Aeroelastic Mode 2 Calculated with the p-k Method

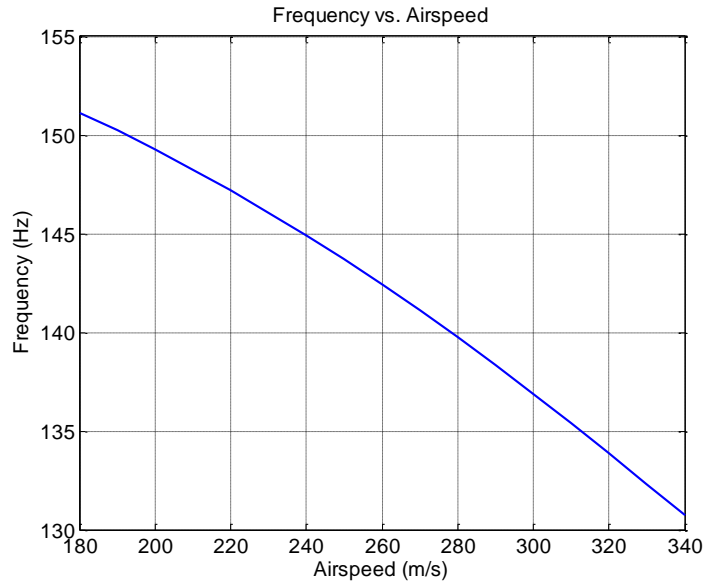


Figure 14 Frequency of Aeroelastic Mode 2 Calculated with the p-k Method

Root Locus Solution:

One way of searching for aeroelastic instability is to analyze \mathbf{A}_{sys} , given in Eqn. (2) for stability. The eigenvalues of \mathbf{A}_{sys} is equivalent to the poles of the aeroelastic transfer function, and these eigenvalues are tracked in the locus of roots diagram, by gradually increasing the free stream speed in q . \mathbf{A}_{sys} has many eigenvalues which involve information about the dynamics of both the aeroelastic generalized coordinates and the aerodynamic lag states. When searching for flutter, one is interested in the stability of the generalized coordinates. Note that the transfer function for the aerodynamic lag states is given in Eqn. (15), and the poles of that transfer function is selected to be on the left hand side of the s-plane, so that the resulting aerodynamic lags do not explicitly bring unstability to the system. Then only the eigenvalues corresponding to the generalized coordinates are plotted on the root locus. The only aeroelastic system matrix that is subjected to the root locus analysis in this study is constructed by utilizing the GAF database at Mach 0.75, at which the flutter analysis was carried out with the p-k method. The eigenvalues corresponding to the generalized coordinates are obtained by using the MATLAB command 'eig' for \mathbf{A}_{sys} at selected free stream speeds which range from 180 m/s to 340 m/s, with 10 m/s intervals. System matrix of a damped system gives complex eigenvalues λ , such that:

$$\lambda_j = -\xi_j \omega_j + i \omega_j \sqrt{1 - \xi_j^2} \quad (19)$$

After each λ_j is obtained from eigenvalue analysis, ξ_j effective damping ratio ξ_j and ω_j undamped natural frequency ω_j are obtained for each aeroelastic mode, where the subscript 'j' denotes an aeroelastic mode. The locus of roots for all aeroelastic modes together is given in Figure 15.

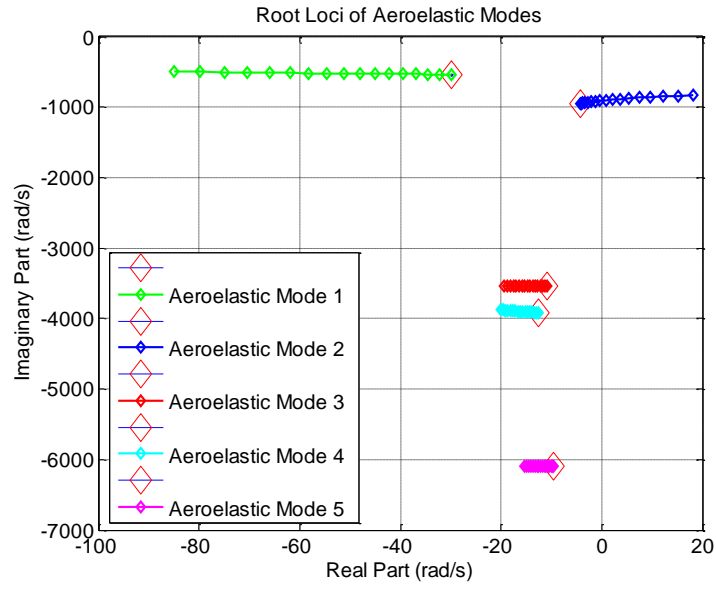


Figure 15 Locus of Aeroelastic Roots

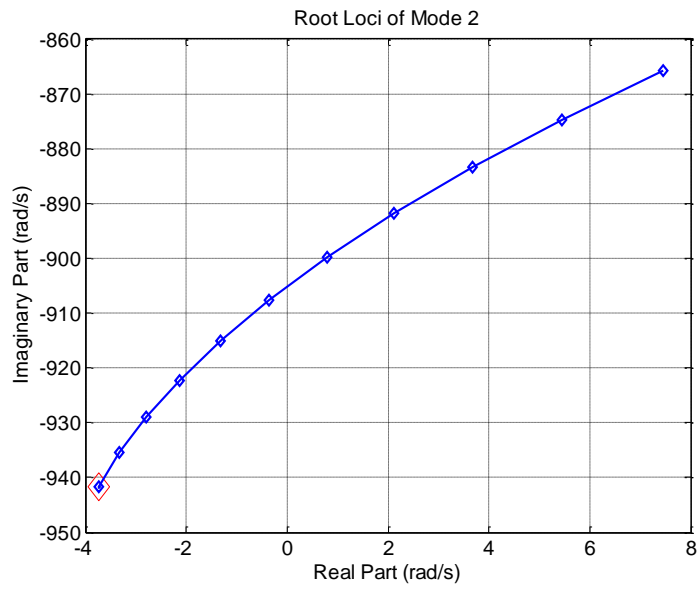


Figure 16 gives the zoomed picture of the aeroelastic roots for aeroelastic mode 2.

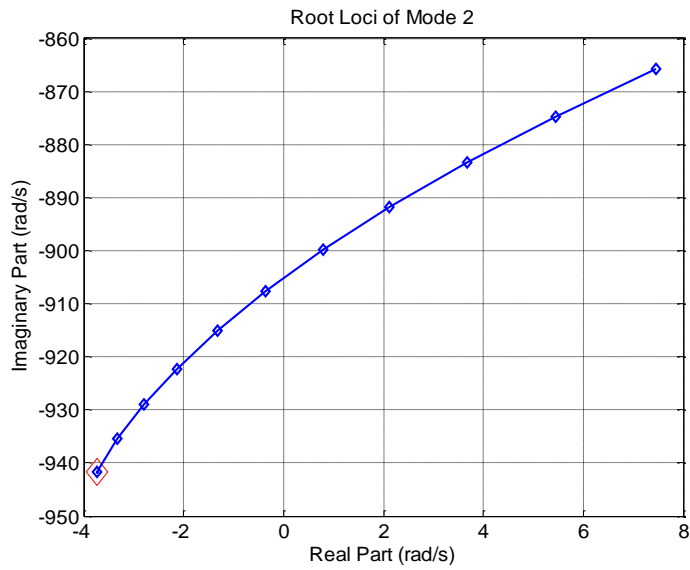


Figure 16 Locus of Aeroelastic Roots for Aeroelastic Mode 2

Since the real part of the aeroelastic roots have positive values as the airspeed increases, instability is found in the second aeroelastic mode. The corresponding damping ratio and natural frequency of the second aeroelastic mode as airspeed changes are given in Figure 17 and Figure 18 respectively.

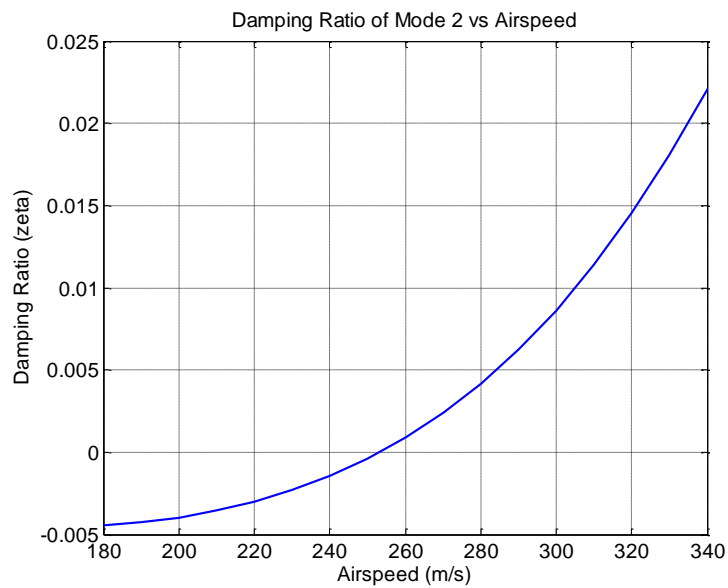


Figure 17 Damping Ratio of Aeroelastic Mode 2 Calculated with the Root Locus Method

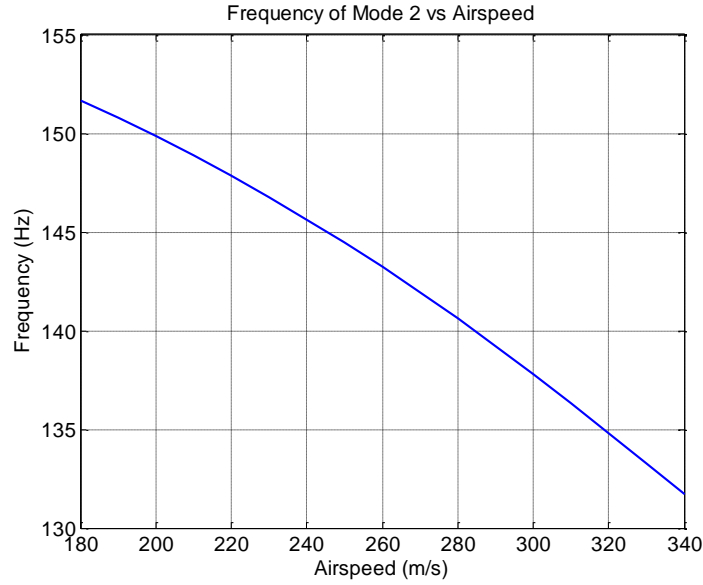


Figure 18 Natural Frequency of Aeroelastic Mode 2 Calculated with the Root Locus Method

The flutter speed is found to be at 253.11 m/s, at which the damping ratio of the second aeroelastic mode is zero. Corresponding to the flutter speed, flutter frequency is obtained as 144.1 Hz. As observed from Figure 15, the only aeroelastic mode that has a positive real part is the second mode. This result is equivalent to the one obtained in p-k method analysis. For the modes analyzed, no mechanism for instability is observed in modes other than the second aeroelastic mode.

Time Domain Solution:

In the present study, time domain solution of flutter is also carried out, so that the aeroelastic system matrix that will be used for the state space analysis is validated. For this purpose, the aeroelastic system matrix constructed with the GAF Database at Mach 0.75 is used. By assigning a unit initial condition to the generalized coordinate of the second aeroelastic mode, time response of the generalized coordinates of the open loop aeroelastic system is simulated with 1 m/s airspeed intervals. Eqn. (21) is integrated with a variable step solver (ode45) built in MATLAB, to obtain the time response of generalized coordinates for the quarter of a second.

$$\{\dot{z}(t)\} = [\mathbf{A}_{sys}] \{z(t)\} \quad (20)$$

In Eqn.(21), the state vector includes aeroelastic generalized coordinates. The initial condition for $z(t)$ is given such that all elements of $z(0)$ is zero except the second aeroelastic generalized coordinate. That initial value is set to unity. Time responses of the generalized coordinate corresponding to the second aeroelastic mode at selected free stream speeds are presented in Figure 19, Figure 20 and Figure 21. From Figs. 19-21, it is seen that flutter speed is approximately 254 m/s, because at 254 m/s, amplitude of oscillations neither decay nor increase.

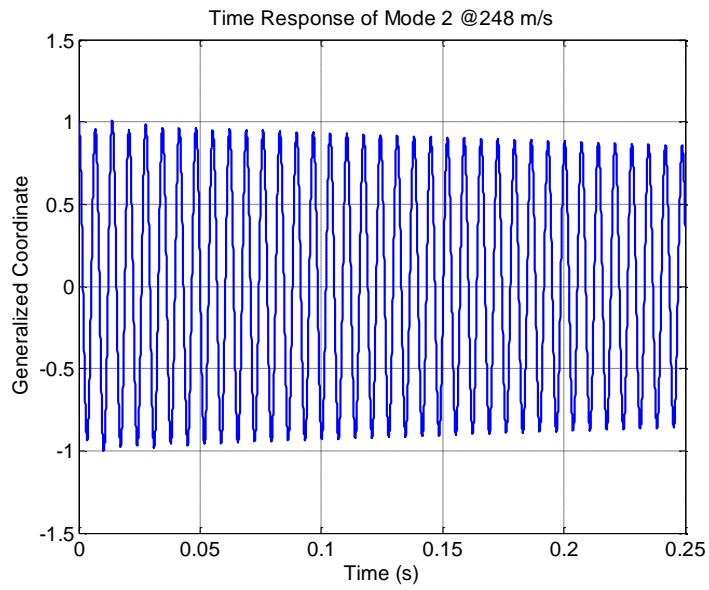


Figure 19 Time Simulation of the Second Aeroelastic Generalized Coordinate at 248 m/s

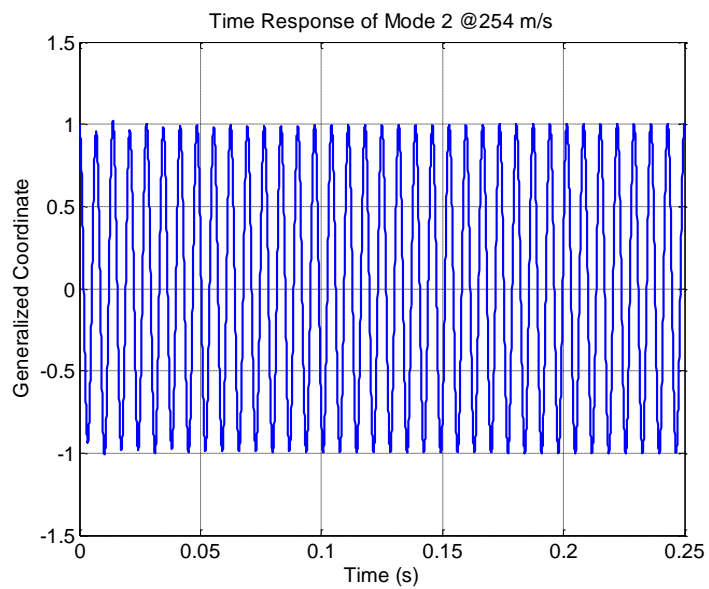


Figure 20 Time Simulation of the Second Aeroelastic Generalized Coordinate at 254 m/s

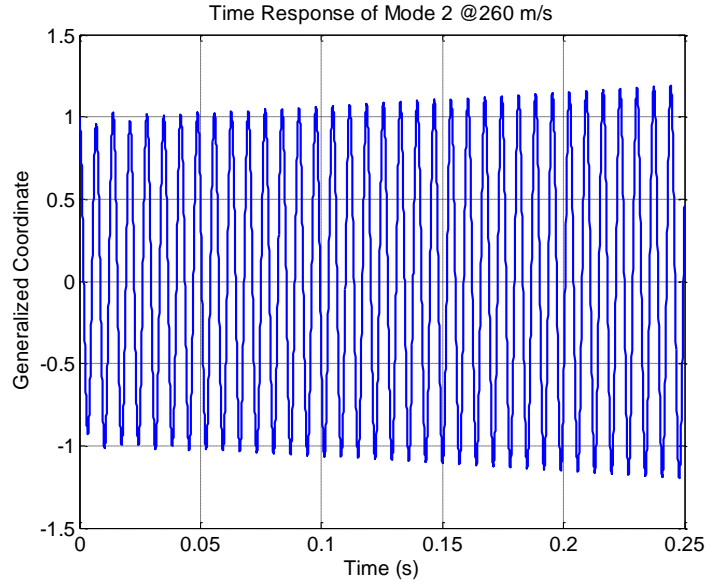


Figure 21 Time Simulation of the Second Aeroelastic Generalized Coordinate at 260 m/s

Comparison of Flutter Solutions

The flutter speeds obtained by three different methods at the sea level are given in Table 5 for comparison.

Table 5 Flutter Speed Comparison

	P-k Method (NASTRAN)	Root Locus Method (MATLAB)	Time Domain Solution (MATLAB)
Altitude (m)	0	0	0
Mach	0.75	0.75	0.75
Air Density (kg/m ³)	1.226	1.226	1.226
Speed of Sound	340.3	340.3	340.3
Flutter Point	Aeroelastic Mode 3	Aeroelastic Mode 3	Aeroelastic Mode 3
Flutter Speed (m/s)	251.12	253.11	254
Flutter Frequency (Hz)	143.55	144.1	-
U^{eq} (m/s)	251.12	253.11	254
M^{eq}	0.74	0.74	0.74

The flutter results presented in Table 5, are considered to be almost identical. Therefore it is concluded that the RFA fitting process and the aeroelastic system matrix construction is valid. Note that U^{eq} and M^{eq} represents the equivalent airspeed and equivalent Mach number, which should match the Mach number used in the analysis.

Servoactuation System Model

In order to fully obtain the models necessary for aeroservoelastic integration and analysis, an electromechanical servo-actuation system with a PD controller is formed. The linear servo-actuation system transfer function which is cascaded with a PD controller including a unity feedback is given in Eqn. (22).

$$\frac{\theta_{fin}}{\theta_{com}} = \frac{K_D K_t s + K_p K_t}{N J L s^3 + N \left(J_{total@motor} R + cL \right) s^2 + \left(N \left(K_b K_t + cR \right) + K_t K_D \right) s + K_p K_t} \quad (21)$$

where θ_{com} is the commanded fin deflection. Note that the aerodynamic hinge moment is not included in Eqn. (21), it is treated as a disturbance to the servo-actuation system. The PD controller of the servo-actuation system is designed using the Root Locus method [Evans, W. R., 1948] by neglecting

the elasticity of the fin and unsteady aerodynamic moment on the fin, as if the fin is rigid and the aerodynamics is steady. The performance requirements of the control fin response, which drive the PD controller design are given in Table 6.

Table 6 Performance Requirements of the Control Fin Response

Settling Time up to 15° Angular Position Command	50 ms
Steady State Angular Position Error	2%
Maximum Load Torque	6 N.m
Minimum Angular Speed at Maximum Load Torque	300°/s

The two primary performance requirements that lead to the determination of the servo-actuation system components, the DC Motor and the transmission unit, are the required torque and the required angular velocity at the fin. The total maximum load torque on the servo-actuator comes from the aerodynamic moment and the acceleration torque due to the inertia of the fin. The stall torque of the actuator should be higher than the resultant of the two. In general, the inertial torque is small relative to the aerodynamic torque, thus neglected in the control design. On the other hand, the size constraints on the actuator unit are demanding in missile applications. A missile is required to be light and compact as possible for any given mission concept, to reduce the costs and improve the dynamic performance. Therefore, strict size constraints are set up on all missile subsystems, including the servo-actuation system. In this case, the DC motor is selected according to a diameter constraint (<28 mm). The DC Motor Specifications are given in Table 7. Since the DC motor is specified, a transmission unit that gives the required maximum torque of 6 N.m is to be selected. No reference to any specific brand or type of transmission is given here. A transmission unit just capable of producing the necessary amount of torque is assumed with following characteristics. The DC motor specifications are given in Table 7. The transmission properties assumed are : $N_{tr} = 66$ $\eta_{tr} = 70\%$ $J_{tr} = 0.5 \times 10^{-7} \text{ kg.m}^2$.

Table 7 DC Motor Specifications

Faulhaber 2642 024CR	
Diameter	26 mm
Length	42 mm
Voltage	24 Volts
Terminal Resistance	5,78 Ohms
Rotor Inductance	550 uH
Torque Constant	34,6 mNm/A
Rotor Inertia	11 g.cm ²

Note that a current limit is implemented through limiting the applied voltage between $(-I_{lim}R, I_{lim}R)$, in addition to a 24V limit for power limited nonlinear simulations.

PD Controller Design

The controller design is carried out in the s-plane with the root locus method. The poles of the open loop actuator transfer function are $s_1 = 0$, $s_2 = -168.80$, and $s_3 = -10340.28$. The root locus method is a good candidate for systems having such dominant pair of poles. The aerodynamic hinge moment is assumed to be an external disturbance, while deriving the actuator transfer function. Therefore the robustness of the closed loop servo-actuation system to the aerodynamic hinge moment is assessed in PD controller design by analysis. No integral control action is preferred, because the open loop actuator transfer function is inherently a Type I system [K. Ogata, 2003], which has zero steady state error. The root locus of the open loop actuator transfer function without the controller near the origin is shown in Figure 22.

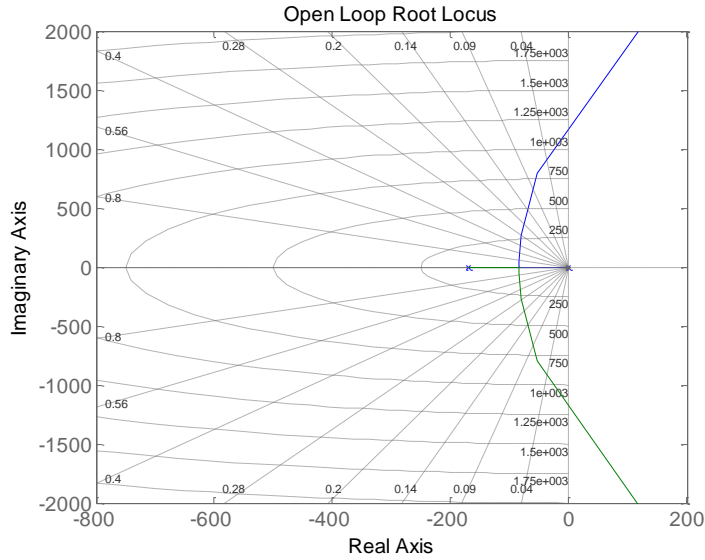


Figure 22 The Open Loop Actuator Root Locus for Dominant Poles

The root locus of the open loop transfer function with the controller is shown in Figure 23, for two different zero locations, both on the left of the second dominant pole $s_2 = -168.806$ of the open loop system, when $K_c = 1$. The zero locations are selected to the left of the second dominant pole so that the system response is adjusted to be faster.

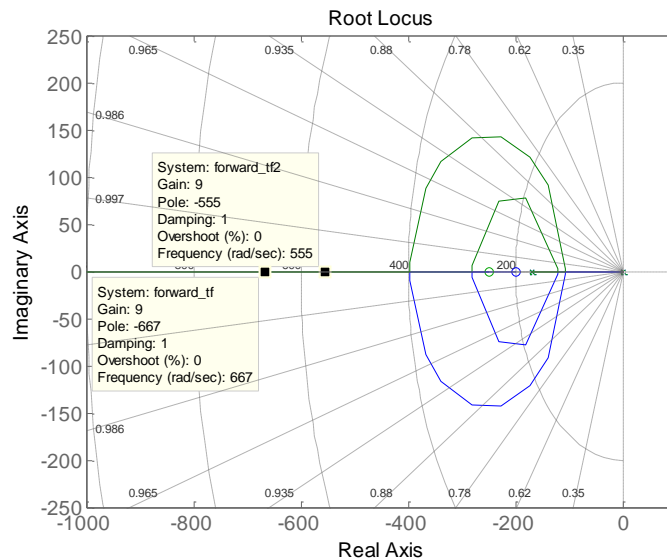


Figure 23 Root Locus of Alternative Compensated Systems

Figure 23 states that, as the controller gain K_c is increased, the system gets faster without becoming unstable. The zeros are placed at $s = -200$ and $s = -250$ respectively. There is always a limit on how much the controller gain K_c can be increased or how far away the zeros can be selected. In general, This limit is due to the hardware implementation of the control system. The operating frequency of the digital control system implemented for the servo-actuation system is assumed to be 1 kHz. Then the fastest dynamic in the controller is selected to be 10% percent of this value for proper operation. Then the limit on the fastest pole is obtained as $s_{\min} \geq -628.32 \text{ rad/s}$.

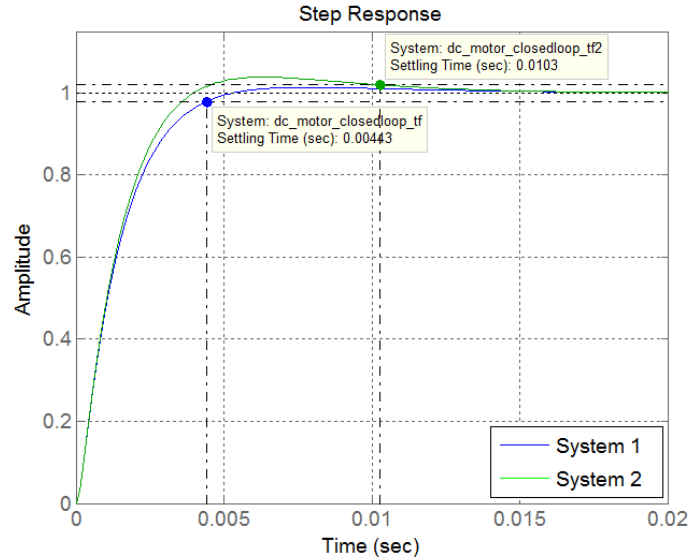


Figure 24 Step Response of Alternative Linear Closed Loop Systems

According to Figure 24, both systems are quite fast, the second one being faster, because the location of the zero is further away on the negative real axis. In the nonlinear system with power source limits, the system that performs faster in linear analysis may be advantageous. Also, it is possible to increase the controller gain K_c further for the second system before reaching the limit s_{min} . The second system with power source limits is simulated to obtain the step response to 14° angular position command and the response is given in Figure 25. The steady aerodynamic hinge moment varying with angular position is applied to the nonlinear system, to check the closed loop system response under anticipated loading conditions.

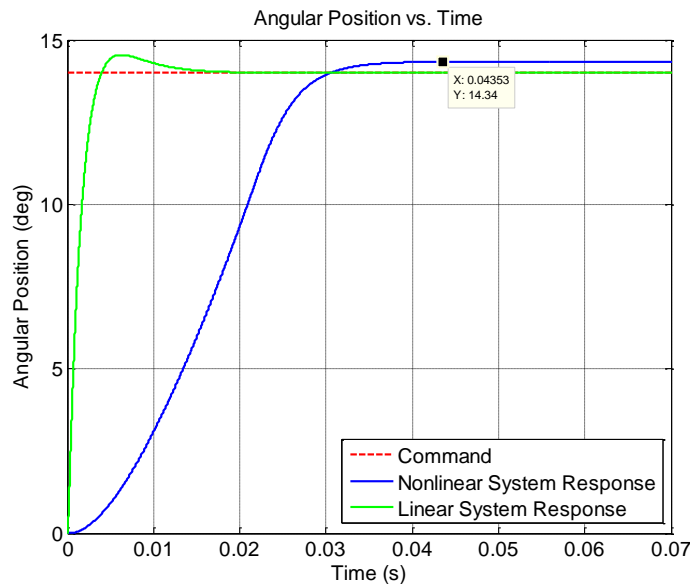


Figure 25 Step Response of System 2 to 14° Command (Linear vs. Power Limited Nonlinear)

Although the system has no overshoot, the steady state error is not acceptable according to the specification which is given as 2%. To meet the 2% requirement the PD controller is tuned such that $K_c = 10$, $K_p = 275$ and $K_D = 1$, and a third system is formed. The step response of System 3 to 14° angular position command is given in Figure 26.

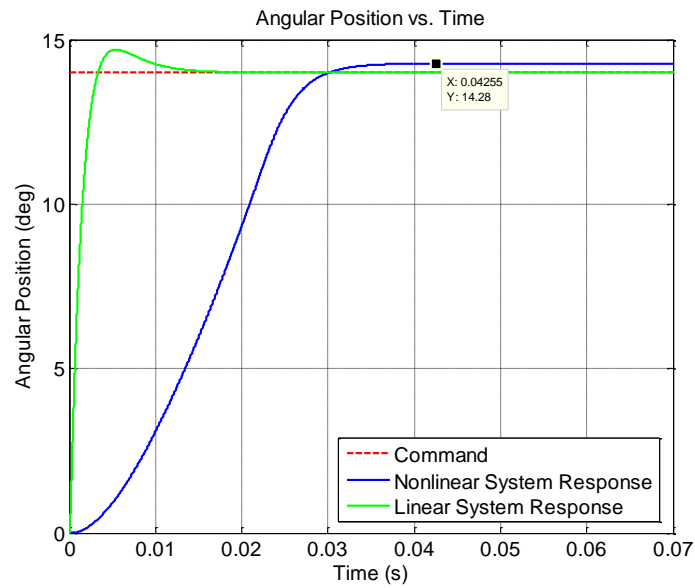


Figure 26 Step Response of System 3 to 14° Command (Linear vs. Power Limited Nonlinear)

Note that, the final system meets the steady state error requirement, settling time requirement and overshoot requirement all together. The steady state error requirement is more demanding than the others, therefore the system turned out to be faster than required. The position, velocity and torque profiles are presented for a -15° command when the initial condition is 15° .

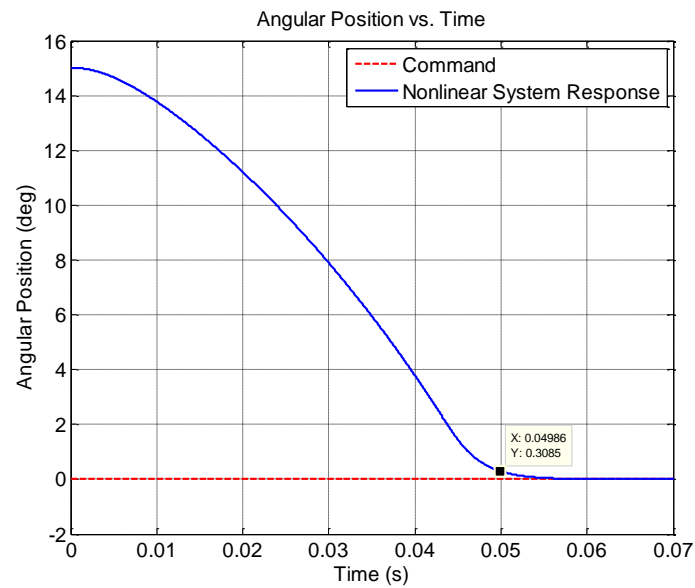


Figure 27 Angular Position Response of the Power Limited Nonlinear System

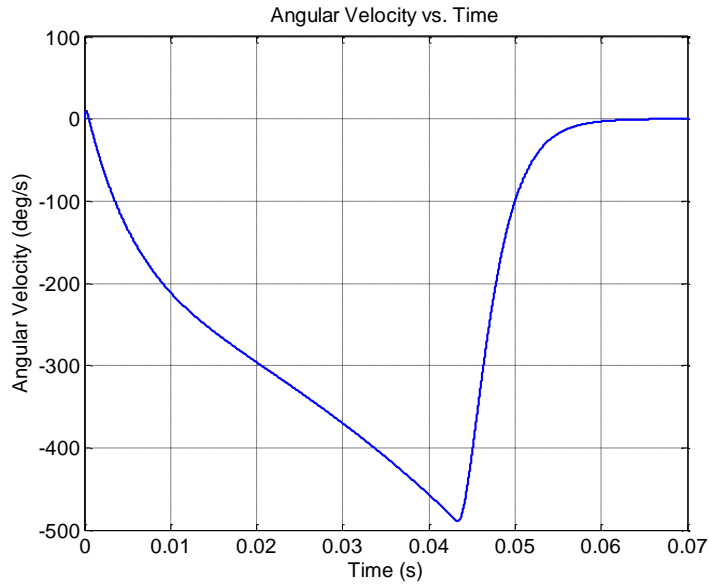


Figure 28 Angular Velocity of the Power Limited Nonlinear System

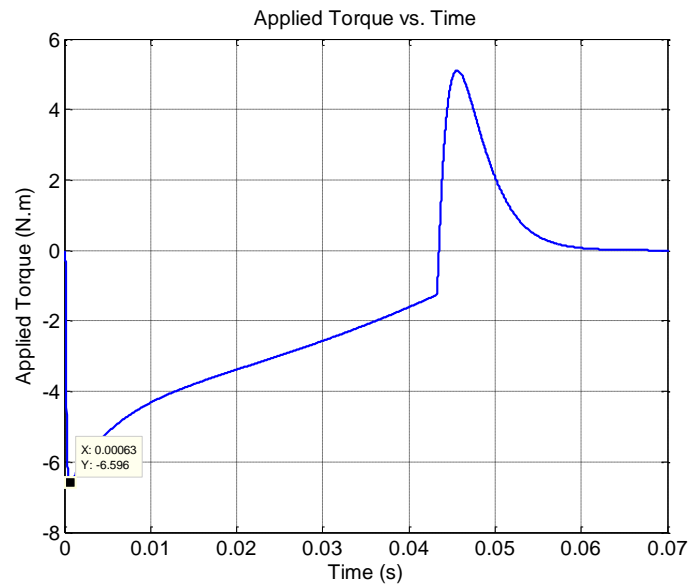


Figure 29 Applied Torque for the Power Limited Nonlinear System

CONCLUSION

This study is focused on presenting structural, aerodynamic and control system models that are to be integrated into an aeroservoelastic missile control fin model, for aeroservoelastic analysis. The modeling methods are intended to include enough genericity, so that they are applicable to design, analysis and control of all-movable control surfaces in an aircraft, although the study is focused on a missile control fin. To provide genericity in structural modeling, the finite element formulation of structural dynamics is utilized. One way of using the practical fictitious mass concept [Karpel, M., and Raveh, D., 1996] is also presented. Aerodynamic modeling is handled with intermediate complexity, by utilizing panel discretization formulation of the Doublet Lattice Method. Panel formulations are still industry standard because of their ease of use, increased fidelity when compared to two dimensional methods and ability to generate fast estimates of linear aerodynamics when compared to CFD methods. Other than the linear unsteady aerodynamic modeling options in MSC Nastran, there are other panel discretization based aerodynamic solvers such as ZAERO, which gives high fidelity representations of unsteady aerodynamic phenomena even when certain linearity assumptions of the

flow is violated. The aerodynamic forces are modeled with Generalized Aerodynamic Force matrices, to introduce additional modularity, since the extraction of these matrices is also possible with higher fidelity CFD solvers. The Generalized Aerodynamic Force matrices are fitted for a range of reduced frequencies with Roger's RFA method, so that the oscillatory aerodynamic forces can be represented in the time domain. Servo-actuation system modeling is carried out by implementing linear and nonlinear power limit phenomena in Matlab.

Flutter analysis and normal modes analysis are carried out for verification of Matlab implementation. It is observed that the results of analysis carried out in MSC Nastran and Matlab are very close, even if different methods such as the p-k method, root locus method and time domain simulation is utilized for flutter analysis.

A controller design scenario with its constraints and requirements is followed, so that an aeroservoelastic model for frequency and time domain analysis could be built. Under the assumptions of steady aerodynamics and a rigid fin, the servo-actuation system is shown to fulfill the performance requirements specified, given the power limit nonlinearity.

References

Bisplinghoff, Raymond L., Ashley, H., Halfman, Robert L., Aeroelasticity. Addison-Wesley Publications, Massachusetts, 1957.

Gülçat, Ü., Fundamentals of Modern Unsteady Aerodynamics, Springer, 2010.

Albano, E., and Rodden, W. P., "A Doublet Lattice Method for Calculating Lift Distributions on Oscillating Surfaces in Subsonic Flow," AIAA Journal, Vol. 7, No. 2, 1969, pp. 279–285.

Luis R. Miranda, Robert D. Elliott, and William M. Baker, A generalized vortex lattice method for Subsonic and supersonic flow applications, NASA CR-2865, December 1977.

Vepa, R., "Finite State Modeling of Aeroelastic Systems," NASA CR-2779, 1977; also, AIAA Paper 76-17, 1976.

Roger, K. L., "Airplane Math Modeling and Active Aeroelastic Control Design," CP-228, AGARD, Brussels, Aug. 1977, pp. 1–11.

Karpel, M., and Hoadley, S. T., "Physically Weighted Approximations of Unsteady Aerodynamic Forces Using the Minimum-State Method," NASATP-3025, March 1991.

Karpel, M., "Reduced-Order Models for Integrated Aeroservoelastic Optimization," Journal of Aircraft, Vol. 36, No. 1, 1999, pp. 146–155.

Nalci, O., Kayran, A., Development Of An Aeroservoelastic Mathematical Model of a Missile Control Fin, 7. ANKARA INTERNATIONAL AEROSPACE CONFERENCE, 11-13 September 2013 - METU, Ankara TURKEY.

Rodden, W.P., and Johnson, E. H., (1994). MSC/NASTRAN Aeroelastic Analysis User's Guide. The MacNeal-Schwendler Corporation.

Reymond, M., MD NASTRAN 2006 DMAP Programmer's Guide, The MacNeal-Schwendler Corporation, 2006.

Anderson, J. D., Fundamentals of Aerodynamics, McGraw-Hill, 3rd edition, January 2001.

Karpel, M., "Design for Active Flutter Suppression and Gust Alleviation Using State-Space Aeroelastic Modeling," Journal of Aircraft, Vol. 19, No. 3, 1982, pp. 221-227.].

Nalci, O., Aeroservoelastic Modeling Of A Missile Control Fin, Master's thesis, Middle East Technical University, 2013.

Evans, W. R., "Graphical Analysis of Control Systems," Transactions of the AIEE, Vol. 67, 1948, pp. 547-551.

K. Ogata, Modern Control Engineering, 4th edition, Pearson Education, New Delhi, 2003.

Karpel, M., and Raveh, D., "Fictitious Mass Element in Structural Dynamics," AIAA Journal, Vol. 34, No. 3, 1996, pp. 607-613.